Raman spectrum of nanocrystals: Phonon dispersion splitting and anisotropy

Bruno P. Falcão,[1,*] Joaquim P. Leitão,[1] Hugo Águas,[2] and Rui N. Pereira[1,3]

[1]*Departamento de Física and I3N, Universidade de Aveiro, Campus Universitário de Santiago, 3810-193 Aveiro, Portugal*

[2]*CENIMAT/I3N, Departamento de Ciência dos Materiais, Faculdade de Ciências e Tecnologia, Universidade Nova de Lisboa, CEMOP-UNINOVA, 2829-516 Caparica, Portugal*

[3]*Walter Schottky Institut and Physik-Department, Technische Universität München, Am Coulombwall 4, 85748 Garching, Germany*

(Received 23 May 2018; revised manuscript received 18 October 2018; published 6 November 2018)

The effects of anisotropy and splitting of the phonon dispersions in the Raman spectrum of nanocrystals are investigated. We describe the different branches of the optical phonon dispersion curves along each high-symmetry direction by fitting a simple empirical model to experimental data. These curves are then used to calculate the Raman spectrum in the framework of the phonon confinement model and the results are compared with a wide range of available experimental data as well as with the spectra predicted by currently available models based on a single isotropic dispersion curve. We show that by considering the anisotropy and splitting of rigorously obtained optical phonon dispersions, the commonly observed deviations between experimental and theoretical data are strongly reduced. Our work enables the extraction of significantly more accurate information about relevant physical properties of nanocrystals from Raman spectroscopy.

DOI: 10.1103/PhysRevB.98.195406

The investigation of the properties of nanomaterials is very challenging due to the differences with their bulk counterparts and the intrinsic limitations of characterization techniques [1–5]. Raman spectroscopy presents significant experimental advantages and can provide a wealth of information in a single spectrum [6–12]. For instance, the size dependence of the photon scattering process in nanomaterials promotes a shift and broadening of the Raman spectrum whose analysis is particularly useful to evaluate the size of nanocrystals or the diameter of nanowires [13–18]. This has been motivating the development of specific theories able to model the Raman spectrum as a function of the nanomaterials properties such as size and shape [19].

The influence of crystal size on the Raman spectrum of nanocrystals has been investigated following three main approaches: the phenomenological phonon confinement model (PCM) [20,21], a continuum theory [22–24], and microscopic lattice dynamical calculations [25–27]. Although the PCM is not the most accurate method to describe the Raman spectrum of nanocrystals, it is the simplest and most practical analytical tool to obtain valuable information from Raman spectroscopy [13,15–21,28,29]. The model is based on the relaxation of selection rule $\vec{q} = 0$ ($\vec{q}$ being the phonon wave vector) imposed by the finite crystal size, enabling the involvement of phonons away from the center of the Brillouin zone in the photon scattering process. According to the formulation of Richter *et al.* [20] and Campbell and Fauchet [21] (RCF model), the intensity of the first order Raman spectrum as a function of frequency ω is given by the product of a Lorentzian function, arising from the dispersion of phonons in an infinite crystal, and a Fourier coefficient $C(0,\vec{q})$, describing the strength of the confinement, integrated over the entire Brillouin zone

$$I(\omega) = \int \frac{|C(0,\vec{q})|^2}{(\omega - \omega(\vec{q}))^2 + (\Gamma_0/2)^2} d^3\vec{q}, \tag{1}$$

where $\omega(\vec{q})$ is an optical phonon dispersion curve and Γ_0 is the natural linewidth of the Raman peak. Since the proposal of the RCF model, several authors have been modifying and improving it in order to achieve more accurate descriptions of the experimental data [17,28–34]. Some of these improvements regard the choosing of appropriate weighting functions and their parameters to define the strength of the confinement particularly at the boundaries of the crystal. The most common weighting functions follow the Gaussian [13,15,20,21,25,29] or the sinusoidal forms [21,25,28,30,34]. Other improvements include a Bose-Einstein probability factor to describe the Raman scattering efficiency and considering a wave packet extended over the nanocrystal size with q limited to the range $[(2\pi - 1)/L\ (2\pi + 1)/L]$, due to the Heisenberg uncertainty principle, instead of a single-phonon wave vector [28,30]. Doğan *et al.* proposed a comprehensive model that considers all these improvements (hereafter denoted as "standard model") in which the Raman spectrum of a spherical nanocrystal with diameter L is defined as [34]

$$I(\omega, L) \propto \int_{2\pi-1}^{2\pi+1} \rho[\omega(Q)] \frac{4\pi Q^2}{\pi L^3} \frac{\left|3\frac{\sin(Q/2)}{\pi^3 Q(4\pi^2 - Q^2)}\right|^2 (\Gamma_0/2)}{[\omega - \omega(Q)]^2 + (\Gamma_0/2)^2} dQ, \tag{2}$$

where $Q = qL$ and $\rho[\omega(Q)]$ represents the Raman scattering efficiency.

In the case of silicon nanostructures, the PCMs are typically applied to the $\vec{q}$ direction [100] assuming an isotropic dispersion function fitted to neutron scattering experimental data of the LO dispersion branch of the bulk material, such as

*bfalcao@ua.pt

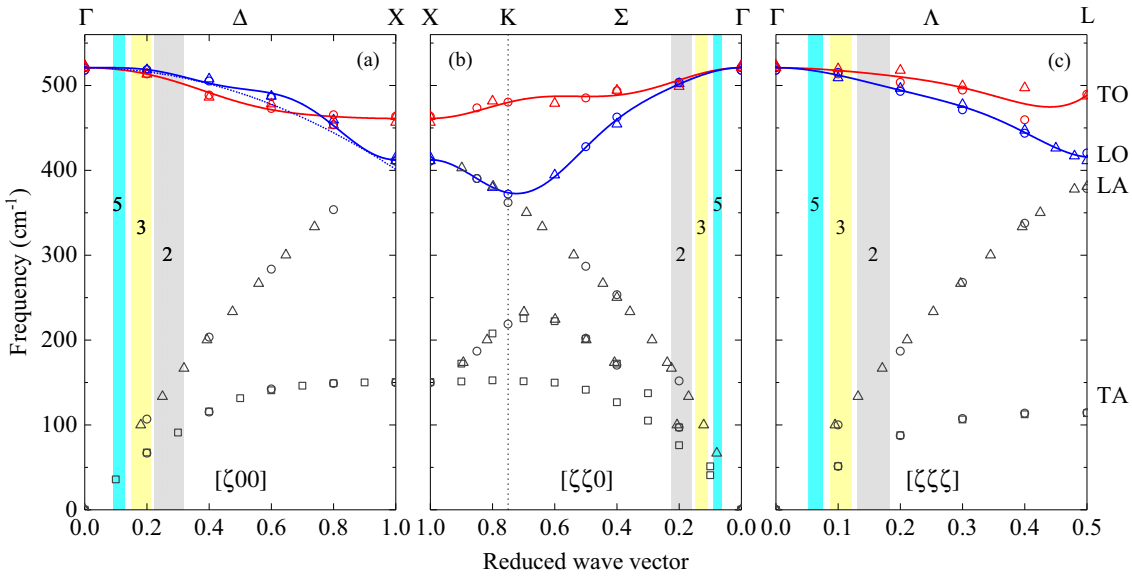

FIG. 1. Phonon dispersion curves of bulk silicon along the high-symmetry directions (a) [100], (b) [110], and (c) [111]. The symbols represent data from the neutron scattering experiments of (circles) Dolling [35], (triangles) Kulda *et al.* [36], and (squares) Nilsson *et al.* [37]. The blue dotted line is the LO phonon dispersion function proposed by Sui *et al.* [38]. The red and blue solid lines are the fitted curves for the TO and LO phonon branches, respectively, from "our model." The vertical shaded areas define the integration ranges of Eq. (2) for a nanocrystal with the indicated diameter L (nm).

the empirical expression $\omega(q) = \omega_0\,(1 - 0.23\,q^2)$ suggested by Sui *et al.* [38], where ω_0 is the natural frequency of the optical phonons at the center of the Brillouin zone (521 cm^{-1}). As shown by the dotted blue line in Fig. 1(a), Sui's expression reproduces fairly well the experimental data (blue symbols) of the LO phonon dispersion along [100]. However, this approach disregards the anisotropy of the LO phonon dispersion, which is evident by comparing the phonon dispersion data along directions [100], [110], and [111] (see Fig. 1). The anisotropy of the LO phonons may not be problematic for large nanocrystals where the confinement effect is negligible, but for small nanocrystals the integral in Eq. (2) receives contributions from the phonon dispersion away from the center of the Brillouin zone, as indicated in Fig. 1 by the shaded areas for sizes $L = 2$, 3, and 5 nm. Consequently, as the nanocrystal size diminishes, more critical is the description of the LO phonon curves away from the Γ point. In order to remove the direction dependence associated with the anisotropy of the optical phonons, Paillard *et al.* proposed an analytical expression derived from the Brout sum rule that involves averaging the different phonon branches along the main $\vec{q}$ directions [28]. In any case, dealing with an isotropic dispersion function such as that given by Sui's expression or averaging data along different directions (Paillard's method) is not a sufficient approach and may work only when the materials do not possess strong anisotropic phonon-dispersion properties [29,32,39]. Another important issue is that none of the above approaches considers the lifting of optical phonons degeneracy (for $q > 0$) and the resulting fact that the LO and TO branches along any direction have quite different dispersions (see Fig. 1). Hence, the contribution of the TO dispersion should also be taken into account to calculate the Raman spectrum. In sum, it is important to consider both the effect of anisotropy and splitting of the optical phonon branches to describe the experimental data for different $\vec{q}$ directions as close as possible, which cannot be done with single isotropic or averaged dispersion curves.

We consider here a purely algebraic approach inspired in the work of Roodenko *et al.* [29] to accurately describe the optical phonons dispersion curves along different directions. Accordingly, each phonon branch is fitted with a Fourier-type expansion up to $n = 4$,

$$\omega(q) = F_0 + \sum_{n=1}^{4} F_n \cos(n\pi q), \tag{3}$$

where F_n are fitting coefficients. Boundary conditions were imposed to assure that at the high-symmetry points Γ and X the phonon curves represented in the different directions have the same value: $\omega(\Gamma) = 521\ \mathrm{cm}^{-1}$, $\omega(X)_{[100]} = \omega(X)_{[110]}$ (see Supplemental Material [40]). The dispersion relations obtained for the TO and LO phonon branches are depicted in Fig. 1 as red and blue solid lines, respectively.

In order to investigate the influence of anisotropy and splitting of the phonon dispersion relations in the simulation of the Raman spectrum, we calculated the spectrum of a silicon nanocrystal with $L = 3$ nm. This approach is denoted hereafter as "our model." Here, we take into account the different dispersion curves fitted by Eq. (3) in each relevant crystallographic direction. The Raman spectrum is given by the sum of different spectral components calculated through Eq. (2) for the three high-symmetry directions, and all their optical phonon branches, considering proper weighting factors according to the number of equivalent directions

$$I(\omega, L)_{\mathrm{total}} = [6\ 12\ 8] \begin{bmatrix} I(\omega, L)_{[100]} \\ I(\omega, L)_{[110]} \\ I(\omega, L)_{[111]} \end{bmatrix}. \tag{4}$$

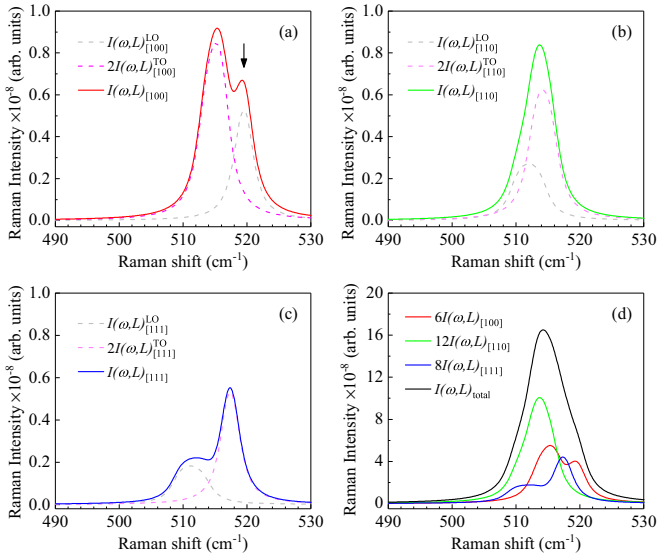

FIG. 2. Raman spectra of a 3 nm silicon nanocrystal resulting from "our model" in the (a) [100], (b) [110], (c) [111] directions, and (d) total spectrum. The weights due to the TO degeneracy and number of equivalent directions are indicated in the legends.

Each term in the second bracket of Eq. (4) is the spectral component calculated through the sum of the LO and TO contributions to the spectrum $I(\omega, L)_{[\ldots]} = I(\omega, L)^{\mathrm{LO}}_{[\ldots]} + 2\, I(\omega, L)^{\mathrm{TO}}_{[\ldots]}$. When evaluating Eq. (2) in the [110] and [111] directions the integration ranges are multiplied by $\sqrt{2}$ and $\sqrt{3}$, respectively, to account for the reduced wave vector representation. The calculations of "our model" are depicted in Fig. 2. The component identified in Fig. 2(a) with an arrow corresponds to the Raman spectrum calculated with the "standard model" (single isotropic dispersion curve). As can be seen in Fig. 2, when the anisotropy of LO phonon branch comes into play there are two additional components from the [110] and [111] directions, which are noticeable redshifted and broadened with respect to that in the [100] direction; compare dashed gray lines in Figs. 2(a)–2(c). Furthermore, the LO and TO phonon splitting leads to the appearance of two spectral components in all directions (dashed gray and red lines in Figs. 2(a)–2(c), respectively). When the anisotropy and phonon splitting effects are taken into account the Raman spectrum [see Fig. 2(d)] becomes much broader and redshifted than that calculated with the "standard model." This clearly indicates the major role played by the phonon splitting and anisotropy in the Raman spectrum simulation.

To test "our model," in the following we compare our simulations with experimental data obtained for free-standing silicon nanocrystals (see Supplemental Material [40] and references therein [34,41–45]). As exemplified in Fig. 3 for one of the samples used in this study, the silicon nanocrystals are characterized by a rather narrow log-normal size distribution $\Phi(L)$, in this case with mean diameter $\bar{D} = 2.9 \pm 0.1$ nm and standard deviation $\sigma = 0.15 \pm 0.02$ nm. The Raman spectrum of these silicon nanocrystals is shown in Fig. 3(b), as well as the corresponding deconvolution based on a fit comprising three Gaussian components (A_i) centered at 330, 444, and 491 cm^{-1} and one Lorentzian curve (B) peaking at 516.5 cm^{-1}. According to previous works, the nature of components A_i can be explained considering surfacelike vibrational modes, where the competing influences of undercoordination, bond length, and quantum effect lowers the vibrational frequencies of the optical phonons [16,46–50]. The peak B is ascribed to the crystalline core of the silicon nanocrystals and is red-shifted and broadened (linewidth $\Gamma \approx 11.5$ cm^{-1}) with respect to the peak observed in bulk silicon.

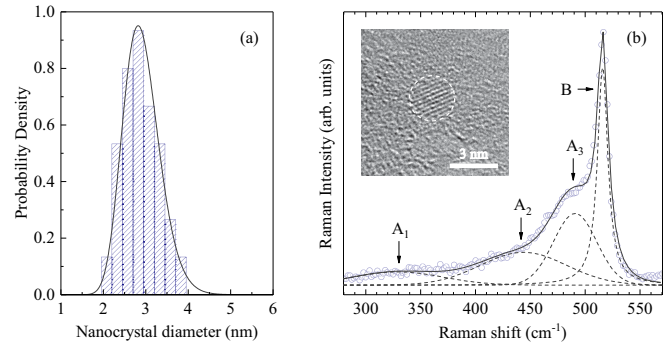

FIG. 3. (a) Size distribution and (b) Raman spectrum of silicon nanocrystals synthesized at 3 Torr. The dashed lines in (b) illustrate the fit to the experimental spectrum assuming three Gaussian (A_i) and one Lorentzian (B) components. The inset in (b) shows a HR-TEM image of a single nanocrystal.

In Fig. 4, we show the comparison of peak B (crystalline contribution), obtained from fitting the experimental spectrum [Fig. 3(b)], with simulations using the "standard model" and "our model." The spectrum simulated by the "standard model," considering $L \equiv \bar{D} = 2.9$ nm, is shown in Fig. 4(a) as a red solid line. As can be seen, the simulated spectrum is significantly narrower than that of component B. Even if the size distribution of the nanocrystals is taken into account, by integrating over the size range $\Phi(L)$ in the following way $I(\omega, \bar{D})_{SD} = \int \Phi(L) I(\omega, \bar{D})\, dL$, the linewidth of the calculated spectrum increases but remains much smaller than

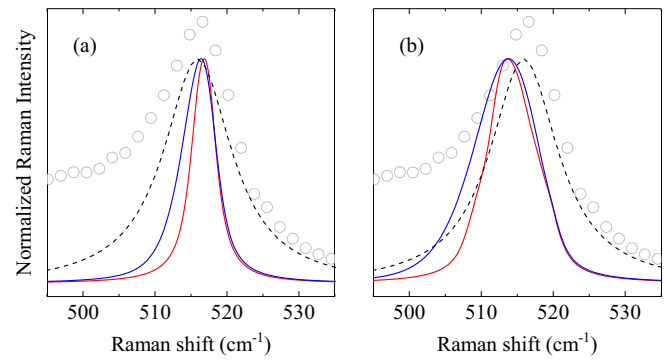

FIG. 4. Comparison between the calculated spectra considering a single nanocrystal size (red lines) and a size distribution (blue lines), with the corresponding fitted component B (dashed line). The theoretical spectra were simulated considering phonon dispersion relations given by (a) the "standard model" and (b) "our model." The circles represent the experimental spectrum.

the experimental one [see blue solid line in Fig. 4(a)]. The investigation of the effects of phonon splitting and anisotropy in the Raman spectrum was performed through the application of "our model" in two steps. First, it was assumed silicon nanocrystals with $\bar{D} = 2.9$ nm, without size distribution [red solid line in Fig. 4(b)]. The comparison of the two red solid lines in Fig. 4 show that the shape of the Raman spectrum is strongly affected by the phonon splitting and anisotropy. Although the peak position of the spectrum calculated with "our model" [red solid line in Fig. 4(b)] evidences a slight deviation relatively to the experimental spectrum (dashed line), the linewidth is much closer to that observed experimentally than that calculated with the "standard model" [Fig. 4(a)]. In the second step, the size distribution was taken into account [blue solid line in Fig. 4(b)]. In this case, the linewidth of the calculated spectrum becomes further closer to that observed experimentally. The comparison of the "standard model" [Fig. 4(a)] with "our model" [Fig. 4(b)], as well as of the spectra simulated with and without size distribution (blue vs red solid lines), indicates that the anisotropy and phonon splitting effects have a more decisive role in the accuracy of the calculated linewidth than the effect of the size distribution.

To gain a broader perspective on the adequacy of "our model," we now compare the trends predicted by "our model" with a wide range of experimental data available in the literature [20,32,51]. In Figs. 5(a) and 5(b) we show the size dependency of the Raman peak position Ω and linewidth Γ, respectively, predicted from "our model" (solid lines) and given by experimental data from the literature (solid symbols) and from our experiments (gray triangles). For comparison we also show the dependencies given by the "standard model" (dashed lines). As can be seen, in general "our model" describes the experimental data considerably better than the "standard model" throughout the whole size range. For sizes below ~2.5 nm, both models are rather inaccurate because the nanocrystals behave like large molecules and the bulklike dispersion relations may no longer remain valid [47,48].

In the literature, the commonly observed deviations between experimental data and results obtained from the "standard model," as well as from other formulations of the PCM, are usually ascribed to (combined) effects of nanocrystal size distribution [32,33,52], laser heating [53–55], and strain [56,57]. However, our study clearly shows that the anisotropy and splitting of the optical phonon dispersion relations, which must be considered in combination with an accurate description of these relations, contribute critically to the size-dependent shifts of Ω and Γ observed for nanocrystals with respect to values of the bulk (dotted lines in Fig. 5). We note that the calculated trends shown in Fig. 5 (solid lines) do not take into account the size distribution of the nanocrystals. However, as mentioned above, the size distribution should have a contribution to Raman spectrum deviations with respect to bulk c-Si smaller than those of the phonon dispersion splitting and anisotropy. The reasonable agreement between the solid lines and experimental data shown in Fig. 5 also gives support to this conclusion. Thus, the relations between the nanocrystal size and Ω (and Γ) determined from "our model" (solid lines in Fig. 5) provide a more accurate practical approach for the nanocrystal size estimation through Raman spectrum parameters (i.e., Ω and Γ) than

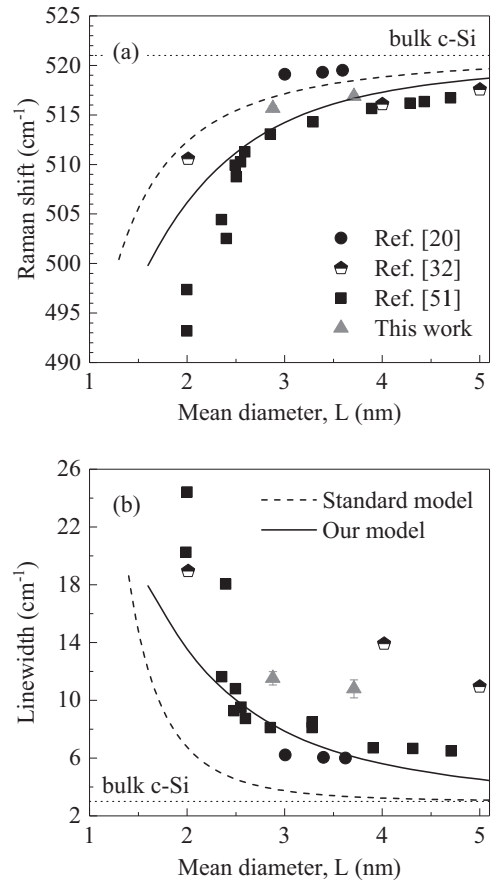

FIG. 5. (a) Raman shift and (b) linewidth as a function of nanocrystal diameter. The dashed and solid lines are the simulations carried with "standard model" and "our model" (single nanocrystal size), respectively. Triangles represent our experimental data for samples with average mean diameter of 2.9 and 3.7 nm (see Supplemental Material [40]), whereas experimental data from several authors are displayed as black symbols. Legends in (a) and (b) complement each other.

those given by the "standard model." This is particularly interesting because in most cases there is no *a priori* information about the size distribution of the nanocrystals being analyzed.

Finally, we note also that care should be taken while simulating the Raman spectrum of nanomaterials for which detailed phonon dispersion relations are unavailable, due to the possible influence of the anisotropy and phonon splitting in the shape of the Raman spectrum. The application of "our model" to nanocrystals of other materials requires that accurate experimental data is available for the phonon dispersion curves. For most materials, such data is not available with the same level of detail as for silicon. This may be a drawback of Raman spectroscopy as a widespread technique for nanocrystal size determination. However, our work may motivate further investigations of phonon dispersion relations in other materials.

In summary, we have investigated the role of anisotropy and splitting of the optical phonon dispersion relations in the Raman scattering of small nanocrystals within the framework of the phonon confinement model. It is shown

that these effects have a much more important contribution to the commonly observed deviations of the Raman spectrum of nanocrystals with respect to their bulk counterparts than has been considered so far. Our work demonstrates that the consideration of these effects enables a more accurate simulation and analysis of Raman spectra of nanomaterials than the currently applied phonon confinement models.

The authors would like to thank José Coutinho for useful discussions and José Daniel Gouveia for his support with the PCM simulations. This work has been developed with the financial support from the Fundação para a Ciência e a Tecnologia (FCT) and FEDER through Projects No. UID/CTM/50025/2013, No. POCI-01-0145-FEDER-007688, and No. PTDC/CTM-ENE/2514/2012.

[1] D. V. Talapin, J.-S. Lee, M. V. Kovalenko, and E. V. Shevchenko, Chem. Rev. **110**, 389 (2010).
[2] J. Y. Kim, O. Voznyy, D. Zhitomirsky, and E. H. Sargent, Adv. Mater. **25**, 4986 (2013).
[3] F. Priolo, T. Gregorkiewicz, M. Galli, and T. F. Krauss, Nat. Nanotech. **9**, 19 (2014).
[4] M. V. Kovalenko, L. Manna, A. Cabot, Z. Hens, D. V. Talapin, C. R. Kagan, V. I. Klimov, A. L. Rogach, P. Reiss, D. J. Milliron, P. Guyot-Sionnnest, G. Konstantatos, W. J. Parak, T. Hyeon, B. A. Korgel, C. B. Murray, and W. Heiss, ACS Nano **9**, 1012 (2015).
[5] C. R. Kagan, E. Lifshitz, E. H. Sargent, and D. V. Talapin, Science **353**, 885 (2016).
[6] M. Grimsditch, J. E. Mattson, C. H. Sowers, S. D. Bader, and M. J. Peters, Phys. Rev. Lett. **77**, 2025 (1996).
[7] H. K. Yadav, V. Gupta, K. Sreenivas, S. P. Singh, B. Sundarakannan, and R. S. Katiyar, Phys. Rev. Lett. **97**, 085502 (2006).
[8] G. Gouadec and P. Colomban, Prog. Cryst. Growth Charact. Mater. **53**, 1 (2007).
[9] D. O. Sigle, J. T. Hugall, S. Ithurria, B. Dubertret, and J. J. Baumberg, Phys. Rev. Lett. **113**, 087402 (2014).
[10] B. P. Falcão, J. P. Leitão, M. R. Correia, M. R. Soares, H. Wiggers, A. Cantarero, and R. N. Pereira, Phys. Rev. B **95**, 115439 (2017).
[11] A. Iskandar, A. Gwiazda, J. Younes, M. Kazan, A. Bruyant, M. Tabbal, and G. Lerondel, Phys. Rev. B **97**, 094308 (2018).
[12] T. Oyake, L. Feng, T. Shiga, M. Isogawa, Y. Nakamura, and J. Shiomi, Phys. Rev. Lett. **120**, 045901 (2018).
[13] P. M. Fauchet and I. H. Campbell, Crit. Rev. Solid State **14**, S79 (1988).
[14] S. Piscanec, M. Cantoro, A. C. Ferrari, J. A. Zapien, Y. Lifshitz, S. T. Lee, S. Hofmann, and J. Robertson, Phys. Rev. B **68**, 241312(R) (2003).
[15] K. W. Adu, H. R. Gutiérrez, U. J. Kim, G. U. Sumanasekera, and P. C. Eklund, Nano Lett. **5**, 409 (2005).
[16] K. H. Khoo, A. T. Zayak, H. Kwak, and J. R. Chelikowsky, Phys. Rev. Lett. **105**, 115504 (2010).
[17] A. C. A. Silva, E. S. F. Neto, S. W. da Silva, P. C. Morais, and N. O. Dantas, J. Phys. Chem. C **117**, 1904 (2013).
[18] L. Han, M. Zeman, and A. H. M. Smets, Nanoscale **7**, 8389 (2015).
[19] A. K. Arora, M. Rajalakshmi, T. R. Ravindran, and V. Sivasubramanian, J. Raman Spectrosc. **38**, 604 (2007).
[20] H. Richter, Z. P. Wang, and L. Ley, Solid State Commun. **39**, 625 (1981).
[21] I. Campbell and P. Fauchet, Solid State Commun. **58**, 739 (1986).
[22] E. Roca, C. Trallero-Giner, and M. Cardona, Phys. Rev. B **49**, 13704 (1994).
[23] C. Trallero-Giner, A. Debernardi, M. Cardona, E. Menéndez-Proupín, and A. I. Ekimov, Phys. Rev. B **57**, 4664 (1998).
[24] M. I. Vasilevskiy, A. G. Rolo, M. J. M. Gomes, O. V. Vikhrova, and C. Ricolleau, J. Phys.: Condens. Matter **13**, 3491 (2001).
[25] J. Zi, K. Zhang, and X. Xie, Phys. Rev. B **55**, 9263 (1997).
[26] H. Fu, V. Ozoliņš, and A. Zunger, Phys. Rev. B **59**, 2881 (1999).
[27] W. Cheng, S.-F. Ren, and P. Y. Yu, Phys. Rev. B **68**, 193309 (2003).
[28] V. Paillard, P. Puech, M. A. Laguna, R. Carles, B. Kohn, and F. Huisken, J. Appl. Phys. **86**, 1921 (1999).
[29] K. Roodenko, I. A. Goldthorpe, P. C. McIntyre, and Y. J. Chabal, Phys. Rev. B **82**, 115210 (2010).
[30] G. Faraci, S. Gibilisco, P. Russo, A. R. Pennisi, and S. La Rosa, Phys. Rev. B **73**, 033307 (2006).
[31] S. K. Gupta and P. K. Jha, Solid State Commun. **149**, 1989 (2009).
[32] V. A. Volodin and V. A. Sachkov, J. Exp. Theor. Phys. **116**, 87 (2013).
[33] I. F. Crowe, M. P. Halsall, O. Hulko, A. P. Knights, R. M. Gwilliam, M. Wojdak, and A. J. Kenyon, J. Appl. Phys. **109**, 083534 (2011).
[34] İ. Doğan and M. C. M. van de Sanden, J. Appl. Phys. **114**, 134310 (2013).
[35] G. Doling, *Inelastic Scattering of Neutrons in Solids and Liquids*, edited by S. Ekland (IAEA, Vienna, 1963), Vol. II.
[36] J. Kulda, D. Strauch, P. Pavone, and Y. Ishii, Phys. Rev. B **50**, 13347 (1994).
[37] G. Nilsson and G. Nelin, Phys. Rev. B **6**, 3777 (1972).
[38] Z. Sui, P. P. Leong, I. P. Herman, G. S. Higashi, and H. Temkin, Appl. Phys. Lett. **60**, 2086 (1992).
[39] I. Gregora, B. Champagnon, L. Saviot, and Y. Monin, Thin Solid Films **255**, 139 (1995).
[40] See Supplemental Material at http://link.aps.org/supplemental/10.1103/PhysRevB.98.195406 for details of the fitting procedure and of the samples and experimental characterization.
[41] H. Hofmeister, F. Huisken, and B. Kohn, Eur. Phys. J. D **9**, 137 (1999).
[42] L. Mangolini, E. Thimsen, and U. Kortshagen, Nano Lett. **5**, 655 (2005).
[43] İ. Doğan, R. H. J. Westermann, K. Dohnalová, A. H. M. Smets, M. A. Verheijen, T. Gregorkiewicz, and M. C. M. van de Sanden, J. Appl. Phys. **113**, 134306 (2013).
[44] L. Han, M. Zeman, and A. H. M. Smets, Appl. Phys. Lett. **106**, 213106 (2015).

[45] J. Knipping, H. Wiggers, B. Rellinghaus, P. Roth, D. Konjhodzic, and C. Meier, J. Nanosci. Nanotechnol. **4**, 1039 (2004).
[46] D. K. Yu, R. Q. Zhang, and S. T. Lee, J. Appl. Phys. **92**, 7453 (2002).
[47] A. Valentin, J. Sée, S. Galdin-Retailleau, and P. Dollfus, J. Phys.: Conf. Ser. **92**, 012048 (2007).
[48] A. Valentin, J. Sée, S. Galdin-Retailleau, and P. Dollfus, J. Phys.: Condens. Matter **20**, 145213 (2008).
[49] Y. Gao, X. Zhao, P. Yin, and F. Gao, Sci. Rep. **6**, 20539 (2016).
[50] Y. Gao and P. Yin, Sci. Rep. **7**, 43602 (2017).
[51] G. Faraci, S. Gibilisco, P. Russo, A. R. Pennisi, G. Compagnini, S. Battiato, R. Puglisi, and S. L. Rosa, Eur. Phys. J. B **46**, 457 (2005).
[52] X. Jia, Z. Lin, T. Zhang, B. Puthen-Veettil, T. Yang, K. Nomoto, J. Ding, G. Conibeerb, and I. Perez-Wurfl, RSC Adv. **7**, 34244 (2017).
[53] R. Gupta, Q. Xiong, C. K. Adu, U. J. Kim, and P. C. Eklund, Nano Lett. **3**, 627 (2003).
[54] K. Adu, Q. Xiong, H. Gutierrez, G. Chen, and P. Eklund, Appl. Phys. A **85**, 287 (2006).
[55] J. Anaya, A. Torres, A. Martín-Martín, O. Martínez, A. C. Prieto, J. Jiménez, A. Rodríguez, J. Sangrador, and T. Rodríguez, Phys. Procedia **8**, 78 (2010).
[56] J. E. Spanier, R. D. Robinson, F. Zhang, S.-W. Chan, and I. P. Herman, Phys. Rev. B **64**, 245407 (2001).
[57] S. Dhara and P. K. Giri, Nanoscale Res. Lett. **6**, 320 (2011).